

Two-dimensional H₂ in Si: Raman scattering and modeling study

V. V. Melnikov*

Tomsk State University, 634050 Tomsk, Russia

M. Hiller and E. V. Lavrov†

Technische Universität Dresden, 01062 Dresden, Germany

(Received 24 January 2018; revised manuscript received 25 February 2018; published 27 March 2018)

Molecular hydrogen trapped within {111}-oriented platelets in silicon is studied by means of Raman scattering and first principles theory. The rotational transition $S_0(0)$ ($J = 0 \rightarrow J = 2$) of para-H₂ (nuclear spin $I = 0$) at 353 cm^{-1} is used as a probe. We find that for temperatures below 100 K the $S_0(0)$ Raman line starts to broaden asymmetrically, which is interpreted as the onset of a phase transition from a state with a short-range order (“gaseous” or “liquid” phase) to a two-dimensional molecular crystal lying in the {111} plane of silicon. The shape of the $S_0(0)$ line at helium temperatures strongly depends on the relative content of ortho- (nuclear spin $I = 1$) and para-H₂ revealing the details of the intermolecular interaction. A comprehensive theoretical analysis based on *ab initio* calculations, molecular dynamics simulations, and rotational spectra modeling reveals that the phase transition to the crystalline state of the two-dimensional hydrogen does occur at temperatures substantially higher compared to those of bulk H₂.

DOI: [10.1103/PhysRevB.97.125307](https://doi.org/10.1103/PhysRevB.97.125307)**I. INTRODUCTION**

Hydrogen is a common and important impurity in semiconductors, which can be trapped at various sites of the host lattice [1]. In Si [2–4], GaAs [5], and Ge [6,7], the introduction of hydrogen in high concentrations results in the formation of extended planar defects, called platelets. In crystalline Si hydrogenated from a plasma at moderate temperatures, these structures are oriented predominantly along {111} crystallographic planes [2,4]. One of the most remarkable properties of these structures is their two dimensionality over diameters of many tens of nanometers while having a thickness of only a few Å [6,8].

Polarization sensitive Raman scattering studies of Si wafers hydrogenated from remote direct current (DC) or radio frequency (RF) plasma revealed the existence of at least two different modifications of {111} platelets, which coexist in concentrations depending on the hydrogenation conditions [4]. At low hydrogenation temperatures, an optically dense structure characterized by a dielectric constant $\epsilon \approx 14$ is formed, whereas for temperatures above 100 °C, a structure with $\epsilon \approx 1$ containing molecular hydrogen dominates [4].

These experimental results are in agreement with theoretical calculations, which find that the double layer of H₂* aggregates has the lowest energy of all proposed models for the {111} platelets [9,10]. For further lattice dilations (higher temperatures), this configuration transforms into the structure where each Si-Si bond in a certain (111) plane is replaced by two Si-H bonds, with H₂ being trapped between the two hydrogenated Si layers [10–12]. At present, this is the most plausible model for the platelets containing molecular hydrogen which will be discussed through this paper.

Molecular hydrogen consists of two protons with nuclear spin $I = 1/2$, thus obeying the Pauli principle requiring the total wave function of the system to be antisymmetric with respect to the permutations of the nuclei. The total nuclear spin of the molecule is either 0, referred to as para-H₂, or 1, referred to as ortho-H₂. Since the nuclear spin wave function of the para (ortho) configuration is antisymmetric (symmetric), the rotational wave function must be symmetric (antisymmetric), thus allowing only even (odd) values for the rotational quantum number J [13].

The conversion from the ortho state with $I = 1$ to the para ground state with $I = 0$ is not possible for an isolated H₂. The presence of an external electromagnetic field, however, renders this transition allowed [14] and it has been observed in various systems such as solid H₂ [15–19], H₂ adsorbed on surfaces [20–23], H₂ in the liquid and gaseous phase [24], as well as inside semiconductor crystals [25–28].

Detailed Raman scattering study of molecular hydrogen trapped within {111}-oriented platelets in silicon were reported in Refs. [4] and [29]. Two platelet types (labeled *A* and *B*) within the “class” of optically “empty” structures with $\epsilon \approx 1$ were identified. They differ in vibrational mode frequencies of the molecule observed at 4143 and 4154 cm⁻¹ (4137 and 4148 cm⁻¹) resulting from two different species of para-H₂ (ortho-H₂). The origin of this difference however remains unveiled.

Independent of the platelet type, the ortho-to-para transition rates were found to be the same within the experimental error bars and equal 0.05 ± 0.03 and $0.08 \pm 0.03 \text{ h}^{-1}$ at 77 and 300 K, respectively. Based on the high density of the hydrogen in platelets, it was proposed that the dominant conversion mechanism is interaction between neighboring H₂ [29].

In addition to the vibrational modes, a set of low frequency Raman lines at 353(1), 587(1), 815(1), and 1034(2) cm⁻¹ was reported and identified as the pure rotational $S_0(0)$,

*melnikov@phys.tsu.ru

†eduard.lavrov@tu-dresden.de

$S_0(1)$, $S_0(2)$, and $S_0(3)$ transitions ($J \rightarrow J + 2$), respectively [29]. In the present study, we get further insight into the properties of two-dimensional hydrogen trapped within $\{111\}$ platelets in Si. State of matter, phase transition, and rotational states are probed by means of Raman scattering and first principles modeling.

II. METHODS

A. Experimental procedure

The samples used in this study were n -type, phosphorous-doped (100) Cz Si wafers with a resistivity of $0.75 \Omega \text{ cm}$. They were hydrogenated in a remote RF (13.56 MHz) plasma at a temperature of about 220°C . The gas pressure was held at 2 mbar.

In order to vary the ortho-to-para ratio of the two H_2 species trapped in the $\{111\}$ platelets, the sample was stored in the dark at 77 K in liquid nitrogen (LN_2) or at $T \leq 20 \text{ K}$ employing liquid helium (LHe). For the para-to-ortho back conversion, the sample was stored in the dark at $300 \pm 1 \text{ K}$ in air.

Raman measurements were performed in a pseudobackscattering geometry using the frequency doubled 532 nm line of a Nd:YVO₄ laser for excitation. For this wavelength, the estimated probing depth $(2\alpha)^{-1}$ is about 410 nm [30]. The incident laser beam made an angle of 40° with the sample normal. The excitation light was focused on a spot size of about $50 \mu\text{m} \times 5 \text{ mm}$ using a cylindrical lens.

The backscattered light was analyzed using a single grating spectrometer and a LN_2 cooled Si CCD detector array. Spectral resolution varied between 2 and 4 cm^{-1} . The measurements were performed with the sample mounted in a cold finger cryostat using liquid helium for cooling.

During the measurements, the temperature in the bulk of the sample, T_b , was varied by an electrical heater. The actual temperature within the excitation area, T_a , however, was different from T_b , and was determined from the Stokes to anti-Stokes ratio of the Si phonon line at 521 cm^{-1} . This allowed us to control temperatures down to approximately 60 K, since for lower temperatures the anti-Stokes intensity was too low to be determined with certainty. For temperatures below 60 K, T_a was estimated by extrapolation of the functional dependence of T_b vs T_a .

The scattering geometry is defined with respect to the (100) sample surface: The x , y , and z axes are parallel to the crystallographic orientations [100], [010], and [001], respectively, whereas the x' , y' , and z' axes are set to be parallel to [100], [011], and $[0\bar{1}1]$, respectively.

In the notation $a(b,c)d$, $a(d)$ refers to the propagation vector of the incident (scattered) light, whereas $b(c)$ characterizes the polarization vector of the incident (scattered) light. The depolarization ratio Δ is defined as the ratio of the intensity of the scattered light polarized perpendicular to the incident light to the intensity of the scattered light polarized parallel to it. In the notation $\Delta_{[xyz]}$, the subscript implies that the excitation light is polarized along the $[xyz]$ axis.

B. Computational details

1. Platelet model

As mentioned in the Introduction, our analysis of the Si $\{111\}$ platelets is based on the formation scenario which

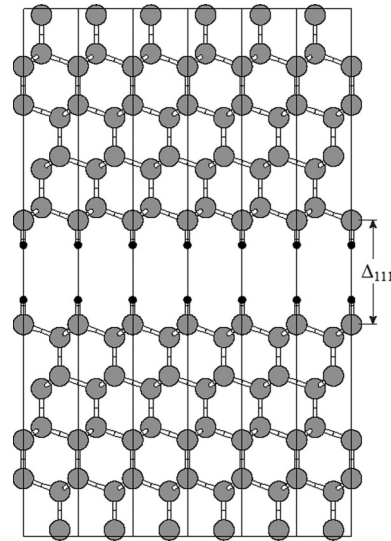


FIG. 1. A Si $\{111\}$ -platelet model projected onto the (110) plane. Si and H atoms are marked by gray and black circles, respectively. The quantity Δ_{111} equals $d_0 + \Delta d$, where d_0 is the Si-Si bond length and Δd is the dilation of the crystal structure.

considers the H_2^* double layer as a precursor [9–12]. The platelet model employed in this study also relies on two important experimental findings.

Firstly, the high-resolution transmission electron microscopy investigations of platelets did not reveal significant distortions of the Si crystalline structure in the vicinity of hydrogen-silicon interfaces, whereby the hydrogen-containing gap in platelets is formed by a lattice dilation of about 3–4 Å [6,8]. Our *ab initio* calculations show that only a Si(111) surface passivated by hydrogen has similar characteristics: Upon passivation of the Si dangling bonds, the interatomic distances between the near-surface layers and those in the bulk of the crystal differ by around 10^{-2} Å . This justifies the representation of the silicon crystal in the platelet's region by its undisturbed atomic structure.

Secondly, according to Raman scattering investigations the values of rotational energy levels ($J \leq 5$) for free and confined H_2 are the same within the experimental error bars [29]. This finding strongly indicates that the interaction between the molecule and the platelet's structure is rather weak; it is also used to verify the adequacy of a theoretical model.

A theoretical treatment of the hydrogen-silicon system was carried out in accordance with the adiabatic approximation. To study the physical properties of Si $\{111\}$ platelets we employed the following model. An H_2 molecule was considered as a rigid diatomic object with the bond length fixed at its average position. The Si crystal was substituted by a static matrix representing the periodic atomic structure. A platelet structure was designed as two Si(111) surfaces passivated by H atoms and separated by dilation of $\Delta d = 4 \text{ Å}$. The Si-H bonds were oriented along the [111] direction with the length fixed at 1.51 Å (see Fig. 1). This approximation is based on the facts that a proton is notably lighter than a silicon atom and an H_2 molecule as well as a Si-H moiety are rigid and quite stable inside the

crystal. In spite of some simplifications, this model provides a reasonably fair description of the system for the temperatures of interest.

The orientational dependence of the interaction between H₂ and the rest of the platelet's structure was neglected. The anisotropy of the hydrogen *intermolecular* interaction was assumed to be due to its electric quadrupole-quadrupole (EQQ) contribution; the isotropic part of the interaction was described by the Lennard-Jones potential (LJ). Other approximations are introduced stepwise at different levels of theory.

In the initial stage of the modeling *ab initio* calculations were carried out to derive the potential energy surface (PES) of the ground electronic state for a set of different configurations of H₂ in a platelet. Preliminarily, test calculations for different magnitudes of the dilation Δd as well as optimization of the platelet's structure were performed to justify consistency of the model.

The data obtained were used to construct an analytic representation of the PES on the basis of pair potentials expansion. Further on, it was employed in molecular dynamics simulations to derive structural, thermodynamic, and kinetic properties of H₂ in platelets. Relying on the results of *ab initio* and molecular dynamics calculations, a quantum mechanical model of two-dimensional H₂ was developed to study the $J = 0$ to $J = 2$ rotational transitions of parahydrogen.

2. *Ab initio* calculations

The adiabatic potential energy surface of the ground electronic state of an H₂ molecule in a Si{111} platelet was calculated using the density functional theory with the PW91 exchange-correlation functional [31] in the generalized gradient approximation [32,33] as implemented in the CRYSTAL09 code [34,35]. Based on the results of previous studies of interstitial molecular hydrogen in silicon [36–38] the same level of theory was used.

The system is treated within the framework of a hexagonal supercell model with periodic boundary conditions and dimensions $(a\sqrt{2}) \times (a\sqrt{2}) \times (3a\sqrt{3} + \Delta d)$ comprising 72 Si and 8 H atoms. Here, a is the silicon lattice parameter. One H₂ molecule is placed in the vacuum gap. The size of the cell is chosen to exclude the interaction of the hydrogen molecule with its periodic images. In the platelet's plane the supercell consists of 2×2 Si(111) surface unit cells. For ease of reading the lattice vectors ($\mathbf{a}/2$, $\mathbf{b}/2$, \mathbf{c}) are used to describe a position within the platelet, i.e., we define the fractional coordinates relative to one Si surface unit cell. Three supercells projected onto the (110) plane are shown in Fig. 1.

In the course of all calculations, the H-H bond was fixed at the equilibrium length and oriented along the [111] direction. The system symmetry was taken into account to select the trial configurations. *Ab initio* energies were obtained for a large number of possible positions of H₂ inside the cell using a $4 \times 4 \times 1$ grid of k points. The basis set by Torres *et al.* [39] for Si and the Dunning DZP basis set [40] for the hydrogen atoms were employed.

3. Molecular dynamics simulations

Molecular dynamics simulations were carried out using the LAMMPS code [41]. To model the time evolution of H₂

in platelets at constant temperature, we employed the Nosé-Hoover thermostat [42,43] and the Velocity Verlet integration with a time step of 1 fs. The system dynamics was considered in the temperature range from 10 to 300 K.

A rectangular supercell with periodic boundary conditions and dimensions $(43a/\sqrt{2}) \times (24a\sqrt{3}/\sqrt{2}) \times (3a\sqrt{3} + \Delta d)$, i.e., approximately $17 \times 16 \times 3$ nm³, was used. The platelet structure was generated by means of the cell constructed at the *ab initio* stage (Fig. 1). To build up a set of initial configurations introduction of hydrogen molecules into the platelet's gap was realized in different ways: randomly, in the vicinity of an equilibrium position, and as a two-dimensional hexagonal lattice. The number of molecules varied from 1032 to 2064. To get insight into the properties of two-dimensional H₂ trapped within platelets, the temperature dependencies of coordinates distribution, radial distribution function (RDF), pressure, specific heat at constant volume, and diffusion coefficient were calculated.

The p - T phase diagram was obtained by investigation of the internal energy, specific heat, and pressure temperature profiles, whereby the pressure of the H₂ subsystem was tuned by changing the concentration of the molecules. The diffusion coefficient was approximated as the slope of the molecule mean-squared displacement versus time.

Structure analysis showed that at low temperatures a two-dimensional crystallization of H₂ occurs. Molecular hydrogen forms a monolayer hexagonal lattice with the parameter $a_{\text{hex}} = a/\sqrt{2}$, i.e., the two-dimensional lattice coincides with the structure of the Si(111) surface. This result was used to develop a quantum mechanical model of solid molecular hydrogen confined within the platelet.

4. Variational calculations of rotational states

The spectral properties of two-dimensional molecular hydrogen crystallized within Si{111} platelets were investigated on the basis of the known properties of bulk solid hydrogen [15,44–50]. Variational calculations of rotational states of two-dimensional H₂ were performed with the ATOMSK toolkit [51].

It is assumed that the temperature of the system does not exceed 50 K, i.e., corresponds to the conditions of the low-temperature Raman scattering measurements (e.g., see Figs. 4 and 5 in Sec. III A). At such temperatures hydrogen molecules are localized mainly in the vicinity of their equilibrium positions which implies that the orientational part of the interaction between H₂ and the rest of the platelet can be disregarded.

It is known that the rotational part of the intermolecular interaction of hydrogen in the solid state has a significant impact on its properties [15,44–48]. According to theoretical estimations [52,53], for example, the energy difference between L and T configurations of an (H₂)₂ dimer is about 27 cm⁻¹ for the center-of-mass distance of 3.7 Å. It is an anisotropic component of the intermolecular potential that is responsible for the splitting of the rotational energy levels in solid H₂ and thus a formation of the rotational energy bands [15,44–48]. Importantly, the main contribution to the anisotropy of the potential comes from the EQQ interaction [15,49].

Still, the splittings of the rotational levels due to the EQQ interaction are small compared to the corresponding rotational energies, which implies that the states with different angular momenta basically do not mix up, i.e., J remains a “good” quantum number.

Two-dimensional H_2 in our model was considered as a hexagonal structure with the lattice parameter a_{hex} . The center-of-mass position of the only basis atom is fixed in the origin of the primitive cell. A supercell with periodic boundary conditions is constructed from the $N = L \times M$ unit cells.

Our Hamiltonian of the system of coupled rotators has the following form:

$$\hat{H} = \sum_i \frac{\hat{\mathbf{J}}_i^2}{2\mu\rho^2} + \frac{1}{2} \sum_{i \neq j} V_{ij}(r_{ij}, \Omega_i, \Omega_j, \Omega_{ij}), \quad (1)$$

where $\hat{\mathbf{J}}_i$ is the angular momentum operator of the i th molecule; ρ is the average H_2 bond length, calculated from $\rho = \hbar/\sqrt{2\mu B_0}$ with the rotational constant of a free molecule $B_0 = 59.322 \text{ cm}^{-1}$ [54], μ is the molecule’s reduced mass. $V_{ij}(r_{ij}, \Omega_i, \Omega_j, \Omega_{ij})$ is the EQQ interaction potential between the i th and j th rotators; r_{ij} is the distance between the center of masses of the two molecules; $\Omega_i \equiv \{\theta_i, \phi_i\}$ are the spherical coordinates of the i th molecule; Ω_{ij} are the spherical coordinates of the i th molecule relative to the j th one. For the two-dimensional lattice $\theta_{ij} = \pi/2$.

The EQQ pair potential is represented as follows [15]:

$$V_{ij} = \Gamma_{ij} 20\pi \sqrt{70\pi} \frac{1}{9} \sum_{t_1, t_2} C(224; t_1 t_2) \times Y_2^{t_1}(\Omega_1) Y_2^{t_2}(\Omega_2) Y_4^{t_1+t_2}(\Omega_{12})^*, \quad (2)$$

where $\Gamma_{ij} = (6/25)e^2 Q^2/r_{ij}^5$ is the EQQ coupling constant; $Q = 0.486 \text{ a.u.}$ [15] is the molecule’s electric quadrupole moment; Y_l^m are the spherical harmonics; $C(224; t_1 t_2)$ are the Clebsch-Gordan coefficients. Only the interaction between the nearest neighbors is taken into account.

The corresponding stationary Schrödinger equation with the Hamiltonian given by Eq. (1) and periodic boundary conditions was solved numerically using the variational approach. The ansatz composed by the products of the spherical harmonics is defined as

$$\psi_n = \sum_{\mathbf{J}} \sum_{\mathbf{m}} U_{\mathbf{J}\mathbf{m}}^n |\mathbf{J}\mathbf{m}\rangle, \quad (3)$$

$$|\mathbf{J}\mathbf{m}\rangle = Y_{J_1}^{m_1}(\Omega_1) Y_{J_2}^{m_2}(\Omega_2) \dots Y_{J_N}^{m_N}(\Omega_N), \quad (4)$$

where $\mathbf{J} = \{J_1, J_2, \dots, J_N\}$; $\mathbf{m} = \{m_1, m_2, \dots, m_N\}$; the summation in Eq. (3) is done over selected \mathbf{J} and \mathbf{m} combination of indices; $U_{\mathbf{J}\mathbf{m}}^n$ are coefficients to be determined by the diagonalization of the Hamiltonian matrix.

The numbers N_o and N_p of ortho- and parahydrogen molecules, respectively, depend on the ortho-to-para concentration ratio $n_o:n_p$ with $N_o + N_p = N$. Only the states with $J \leq 2$ are allowed to be occupied. It is assumed that only one of all para- H_2 molecules can occupy the $J = 2$ state. In this case the indices in Eqs. (3) and (4) obey the condition $\sum J_i \leq 2$, if summed over all even J_i values.

The positions of orthohydrogen are selected in a random way. One function $Y_1^{m_i}(\Omega_i)$ corresponds to the i th ortho- H_2

molecule, where m_i is chosen randomly from the set $\{-1, 0, 1\}$ at the initialization step. The idea is to consider a parahydrogen subsystem embedded in a kind of orthohydrogen bath with the homogeneous distribution of the $\{Y_1^{m_i}\}$ states. Obviously, such a stochastic approach requires a rather large supercell.

Within the framework of our model the quantity $|U_{\mathbf{J}\mathbf{m}}^n|^2$ introduced in Eq. (3) is the probability of finding the system in the $|\mathbf{J}\mathbf{m}\rangle$ state as defined in Eq. (4). The expansion coefficients $U_{\mathbf{J}\mathbf{m}}^n$ can be written as $U_{\mathbf{J}\mathbf{m}}^n = U_{\mathbf{J}\mathbf{m}}^n(\mathbf{R}_i)$, where \mathbf{R}_i are the coordinates of the molecule’s center of mass. The last expression denotes that the excited $|\mathbf{J}\mathbf{m}\rangle$ state corresponds to the $J = 0 \rightarrow J = 2$ transition of a molecule located at \mathbf{R}_i . Thus, $U_{\mathbf{J}\mathbf{m}}^n(\mathbf{R})$ is the wave function of a rotational excitation in the two-dimensional crystal.

In the case of small concentrations of orthohydrogen ($N_p \gg N_o$) the translational symmetry of the system plays a significant role. At such conditions, the delocalized rotational excitations (angular momentum waves) may also occur as a result of the anisotropy of the intermolecular interaction [44].

These waves are characterized by certain values of J and the wave vector \mathbf{k} , which allows us to expand $U_{\mathbf{J}\mathbf{m}}^n$ in Eq. (3) in a series of plane waves

$$U_{\mathbf{J}\mathbf{m}}^n = U_{\mathbf{J}\mathbf{m}}^n(\mathbf{R}) = \sum_{\mathbf{G}} A_{\mathbf{J}\mathbf{m}}^{n\mathbf{k}}(\mathbf{G}) \exp[i(\mathbf{k} + \mathbf{G})\mathbf{R}], \quad (5)$$

where \mathbf{G} are the reciprocal lattice vectors and \mathbf{R} are the coordinates of the lattice sites. Since in Raman scattering the wave vector of the incoming photon is much less than that at the edge of the Brillouin zone, only the states in the vicinity of the Γ point of the rotational band can be probed. Equation (5) is used to select the appropriate delocalized rotational states.

Four cases were considered: pure parahydrogen, a system with 5% of ortho- H_2 ($n_o:n_p = 1:19$), $n_o:n_p = 2:2$, and $n_o:n_p = 3:1$. The supercell size was varied in order to have a comparable number of para- H_2 molecules for each ortho-to-para ratio. The rotational states of the $n_o = 0.05$ system were calculated using a 50×50 cell with $N_p = 2375$. In the case of $n_o:n_p = 2:2$ the computational cell was constructed from 70×70 units with $N_p = 2450$. For the $n_o:n_p = 3:1$ system a 100×100 cell with $N_p = 2500$ was employed.

Since our model comprises a limited number of hydrogen molecules N , the number of calculated rotational states N_{rot} is finite. Therefore the density of states was estimated by means of a statistical analysis of the rotational energy values distribution and represented as $\Delta N_{\text{rot}}/N_{\text{rot}}$ vs E_{rot} with the number of states ΔN_{rot} lying in the energy range $[E_{\text{rot}}, E_{\text{rot}} + \Delta E_{\text{rot}}]$.

If the platelet structure is taken into account, the pure two-dimensional parahydrogen crystal has the C_{3v} symmetry. Hence, the spherical harmonics $Y_J^m(\Omega)$ are classified in accordance with irreducible representations of the C_{3v} point group as $Y_0^0 \in A_1$, $Y_2^0 \in A_1$, $Y_2^{\pm 1} \in E$, and $Y_2^{\pm 2} \in E$.

It was previously established that the electric field of the excitation laser within the platelet is aligned parallel to the [111] direction, i.e., along the Z axis [29]. It follows from here that only the α_{ZZ} component of polarizability is active in the Raman scattering. Since $\alpha_{ZZ} \in A_1$ the $J = 0 \rightarrow J = 2$ transition should obey the rigorous selection rule $A_1 \rightarrow A_1$, i.e., $\Delta J = 2$, $\Delta m = 0$.

The intensities of the Raman transitions were estimated within the framework of the independent polarizability

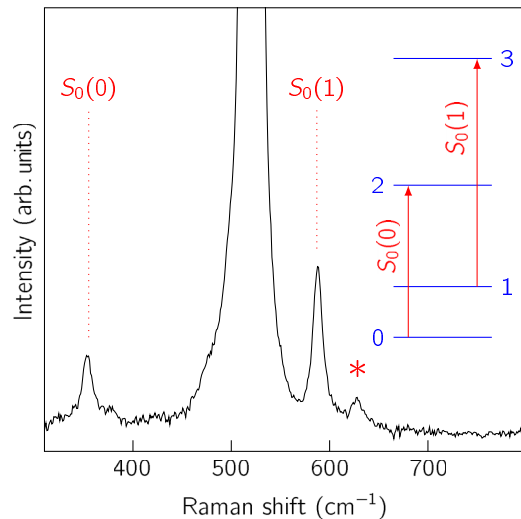


FIG. 2. Raman scattering spectrum taken at room temperature on a (100)-Si sample after exposure to a hydrogen plasma. The spectrum is background corrected by subtracting the spectrum of a virgin Si sample. The line denoted by an * is not related to the hydrogen platelets. Inset shows the energy level diagram of the rotational states of free H₂ together with the corresponding Raman transitions.

approximation when the total polarizability is expressed as the sum of the polarizabilities of free H₂ [50]. The Raman scattering cross section per molecule for the $\psi_0 \rightarrow \psi_n$ transition is defined by

$$\sigma_{ZZ}(n) = \frac{1}{N_p} |\langle \psi_n | \alpha_{ZZ} | \psi_0 \rangle|^2. \quad (6)$$

Thus the integrated intensity should be proportional to

$$I(n) \sim (\omega_s/c)^4 n_p \sigma_{ZZ}(n), \quad (7)$$

where ω_s is the frequency of scattered radiation. The matrix elements in Eq. (6) were calculated using the polarization tensor of H₂ derived in Ref. [50].

III. RESULTS AND DISCUSSION

A. Raman scattering

Figure 2 shows a Raman scattering spectrum taken at room temperature on a (100)-Si sample after exposure to a hydrogen RF plasma at 220 °C. The spectrum was background corrected by subtracting the spectrum of an untreated sample. The line marked by an asterisk is not related to the hydrogen platelets and appears as a result of nonideal subtraction. The Raman phonon transition at around 521 cm⁻¹ dominates the spectrum. The lines positioned at 353 and 587 cm⁻¹ labeled $S_0(0)$ and $S_0(1)$, respectively, are the topic of this study. They are due to the rotational $J = 0 \rightarrow J = 2$ (para-H₂) and $J = 1 \rightarrow J = 3$ (ortho-H₂) transitions of hydrogen trapped within {111} platelets [29]. Corresponding vibrational $Q_1(J)$ modes of H₂ are located at around 4150 cm⁻¹. An in-depth consideration of their properties was presented earlier in Ref. [29]. Here, the $Q_1(J)$ modes will not be discussed.

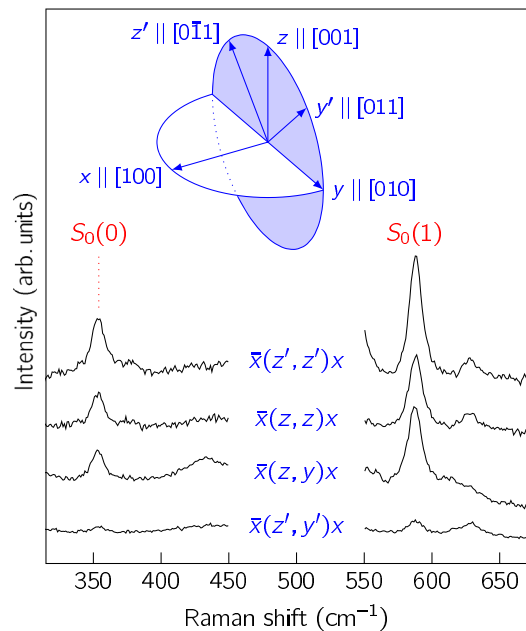


FIG. 3. Polarization sensitive Raman scattering spectra taken at room temperature on a (100)-Si sample after exposure to a hydrogen plasma. The spectra are background corrected by subtracting the spectrum of a virgin Si sample and offset vertically for clarity. Inset shows the measurement geometry.

The rotational energy of a diatomic molecule with rotational quantum number J is given by [13]

$$E_J = \frac{\hbar^2}{2\mu r^2} J(J+1) \equiv BJ(J+1), \quad (8)$$

where μ is the reduced mass and r is the internuclear spacing. The energy of the $S_0(0)$ transition is then $E_{0 \rightarrow 2} = 6B$, whereas for the $S_0(1)$ transition it equals $E_{1 \rightarrow 3} = 10B$. From here we get that for hydrogen in platelets $B = 58.7$ cm⁻¹, which is basically identical to that of free H₂ [55]. We take this as an indication that at room temperature hydrogen in platelets behaves as a free rotator and may be considered as a two-dimensional “gas.”

Figure 3 shows polarization sensitive Raman spectra taken on the $S_0(0)$ and $S_0(1)$ rotational modes. It is obvious from the figure that the depolarization ratio Δ of the two modes depends on the measurement geometry: It is close to zero for the excitation light polarized along the $[0\bar{1}1]$ axis of the crystal ($\Delta_{[0\bar{1}1]} \approx 0$), whereas for the $[001]$ direction $\Delta_{[001]} \approx 1$. Such a behavior implies a trigonal symmetry of the scatterers [56] and complies with the $\{111\}$ orientation of the platelets.

On the other hand, the energies of the $S_0(J)$ modes strongly suggest that H₂ is not aligned with the platelet’s normal and should be considered as a free rotator, which agrees with the conclusions of theory. [10,11] This, in turn, implies that the depolarization ratio of the $S_0(J)$ Raman lines should be close to 3/4 regardless of the measurement geometry [57].

The apparent discrepancy between theory and the polarization properties of the $S_0(J)$ lines is explained by the difference in the dielectric constants between the bulk semiconductor ($\epsilon \approx 14$) and that of the “optically empty” platelet hosting the hydrogen “gas” ($\epsilon \approx 1$) [4,7]. Such a “sandwich”-like structure

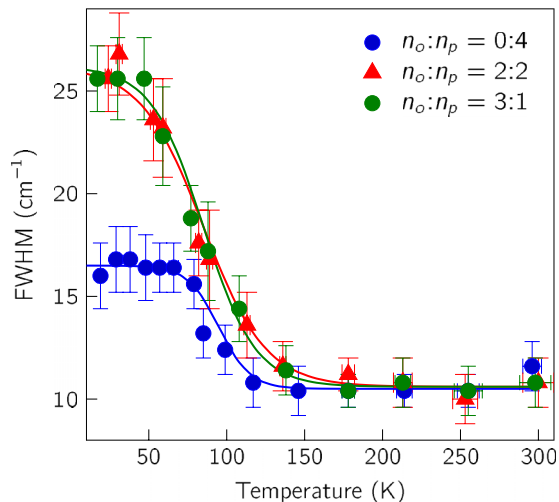


FIG. 4. Full width at half maximum of the $S_0(0)$ Raman transition as a function of temperature obtained for different ortho-to-para ratios. Solid lines are a guide to the eye.

with different ϵ 's results in the preferential orientation of the E vector of the excitation laser light parallel to the platelet's normal and hence—in a trigonal symmetry of the *effective* Raman tensor of freely rotating H_2 in the laboratory frame [29].

The concentration ratio of ortho- and para- H_2 in thermal equilibrium is obtained from

$$\frac{n_o}{n_p} = 3 \frac{\sum_{J=1,3,\dots} (2J+1) \exp(-E_J/kT)}{\sum_{J=0,2,\dots} (2J+1) \exp(-E_J/kT)}. \quad (9)$$

Here, $n_{o(p)}$ denotes the concentration of ortho- H_2 (para- H_2), whereas the prefactor of 3 accounts for the ratio of the degeneracies $(2I+1)$ of the $I=1$ and $I=0$ nuclear spin states. The summation in the numerator is taken over all odd values of J , whereas that of the denominator runs over all even values of J .

The spectra presented in Figs. 2 and 3 were recorded at room temperature. From this temperature on, the ortho-to-para ratio saturates to the value of 3:1 given by the degeneracies of

the two nuclear spin states. In order to get more insight into the properties of hydrogen trapped within platelets it would be, however, desirable to vary the concentration ratio of the ortho and para species. This can be achieved if the sample is kept long enough at the corresponding temperature. For the sake of convenience, these were chosen to be 77 K and $T \approx 20$ K—the temperatures provided by liquid nitrogen and helium at atmospheric pressure, respectively [29]. Note that the sample was not stored directly in LHe bath, since at 4.2 K the conversion time would be impractically long.

From Eq. (9) one obtains that the ortho-to-para ratios at these temperatures are close to 2:2 and 0:4, respectively. Importantly, the back conversion at room temperature to the equilibrium value of 3:1 takes place on the time scale of a few hours providing enough time for mounting the sample into the Raman cryostat without significantly affecting the concentration ratio between the ortho- and para- H_2 [29].

Figure 4 shows obtained full width at half maximum (FWHM) of the $S_0(0)$ line as a function of temperature for the ortho-to-para ratios of 3:1, 2:2, and 0:4. From room temperature down to approximately 150 K the $S_0(0)$ line is insensitive to the relative concentration of the two species. Its FWHM is close to 10 cm^{-1} . Starting from about 140 K the $S_0(0)$ line begins to broaden until it reaches a steady value at about 60 K. We interpret the broadening as the onset of a phase transition of hydrogen from a state with a short-range order to a two-dimensional molecular crystal lying in the $\{111\}$ plane of silicon. This suggestion will be justified theoretically further on in Sec. III B.

Interestingly, the temperature behavior of the $S_0(0)$ line below 150 K significantly depends on $n_o:n_p$. In the case of “pure” para hydrogen, its FWHM is about a factor of two less compared to both “mixed” cases. This strongly indicates that the dominant mechanism of the line broadening is an interaction between neighboring molecules rather than that between H_2 and the Si lattice.

This can be seen more clearly in Fig. 5 which shows temperature dependent Raman spectra taken for the three values of $n_o:n_p$. It follows from the figure that not only the line width but also its shape is sensitive to the neighborhood of para- H_2 .

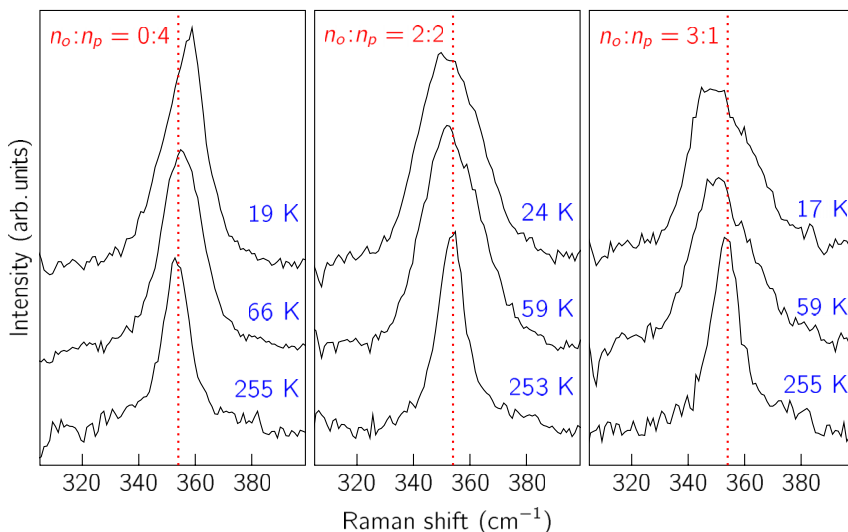


FIG. 5. Temperature dependent Raman scattering spectra taken for an $S_0(0)$ transition of para- H_2 for different ratios between the ortho- and paraspecies. The spectra are offset vertically for clarity.

TABLE I. FWHM (cm⁻¹) and asymmetry (see text) of the S₀(0) Raman line for different ortho-to-para ratios.

| $n_o : n_p$ | A | 254 ± 1 K | | 20 ± 3 K | |
|-------------|---|--------------------------|------|--------------------------|---|
| | | FWHM (cm ⁻¹) | A | FWHM (cm ⁻¹) | A |
| 3:1 | 0 | 10.4 ± 0.8 | 0.3 | 25.6 ± 1.6 | |
| 2:2 | 0 | 10.0 ± 1.2 | 0.1 | 25.6 ± 1.6 | |
| 0:4 | 0 | 10.4 ± 0.8 | -0.4 | 16.0 ± 1.6 | |

In order to describe this effect quantitatively, we introduce the asymmetry of a spectroscopic line defined as

$$A = \frac{\Delta\omega_+ - \Delta\omega_-}{\Delta\omega}, \quad (10)$$

where $\Delta\omega$ is its FWHM, whereas $\Delta\omega_+$ and $\Delta\omega_-$ are the absolute values of differences between the frequency at the maximum intensity (ω_0) and those at the half maximum on the high and the low frequency sides of ω_0 , respectively. Apparently, $\Delta\omega = \Delta\omega_+ + \Delta\omega_-$. The results are gathered in Table I for two temperatures from the opposite sides of the transition region.

It follows from the table as well as Fig. 5 that not only the absolute value of A but also its sign changes as the relative content of para-H₂ grows in. For $n_o:n_p = 3:1$ the maximum of the S₀(0) line is redshifted relative to the frequency detected at 254 ± 1 K, whereby the line shape is asymmetric with $A \approx 30\%$; in the case of equal contents of ortho- and para-H₂ ($n_o:n_p = 2:2$) the S₀(0) line is practically symmetric, and finally, if para-H₂ dominates ($n_o:n_p = 0:4$) ω_0 blueshifts resulting in a negative value of $A \approx -40\%$.

B. Calculations

1. Potential function

To construct an analytic representation of the PES the *ab initio* calculations were carried out for 350 selected nonequivalent positions of H₂ in the platelet. For the purpose of visualization and analysis all symmetry equivalent configurations were generated as well.

The equilibrium position of an H₂ molecule turned out to be located close to the middle of the platelet gap above the Si atom of the second surface layer (excluding the passivation H atoms), i.e., approximately at the (1/3 2/3 1/2) and (2/3 1/3 1/2) points. The only displacement is about 0.05 Å along the [111] axis in the direction from the nearest second layer silicon atom. Thus there are two equilibrium positions relative to the Si(111) surface unit cell.

A contour plot of the PES in the XY plane for $\Delta Z = 0$ is shown in Fig. 6. The X and Z axes of the Cartesian coordinate system XYZ coincide with the lattice vectors **a** and **c**, respectively. The molecule displacements (ΔX , ΔY , ΔZ) are defined relative to the (2/3 1/3 1/2) site. The isoenergetic contours are plotted for the values of 100, 200, and 500 cm⁻¹, and the rest at steps of 500 cm⁻¹. The height of the potential barrier between two nearest minima (saddle point) is about 127 cm⁻¹. Relative to the global minimum, the maximum energy value in the plane is approximately 3820 cm⁻¹ and corresponds to the location of H₂ exactly between the Si-H

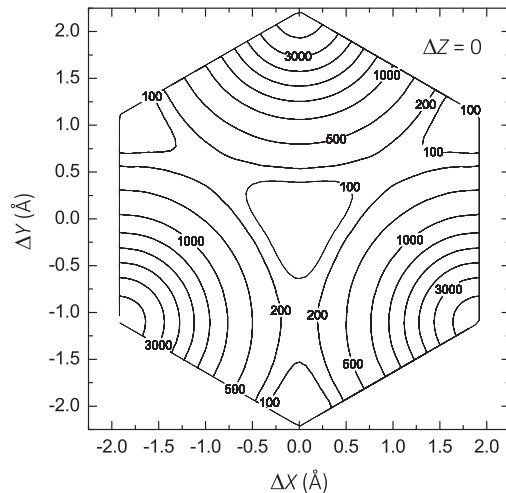


FIG. 6. The potential energy surface of H₂ in the platelet structure plotted for fixed $\Delta Z = 0$. The displacements (ΔX , ΔY , ΔZ) are defined relative to the (2/3 1/3 1/2) position here. Isoenergetic contours are plotted for the values of 100, 200, and 500 cm⁻¹, and the rest at steps of 500 cm⁻¹.

units of the opposite Si surfaces. One can see that the PES properties are largely determined by the interaction of the hydrogen molecule with the Si-H surface terminations.

It should be emphasized that the *ab initio* data allow us to probe only the details of interaction between a *single* H₂ molecule with an “empty” platelet. Filling the platelet with hydrogen should lead to enhancement of the potential barriers, thereby reducing the number of possible diffusion channels. Moreover, taking into account the nature of intermolecular interaction, it is reasonable to assume that upon “filling” the platelet with H₂ the molecules do not occupy the nearest lattice sites. The distance between them is rather short and equals approximately 2.22 Å. On the other hand, the next neighbor spots are determined by the Si(111) surface unit cell, i.e., $a_{\text{hex}} \approx 3.84$ Å. This value is close to the mean distance of approximately 3.79 Å between the molecules in the solid state [15].

The potential energy surface was represented as an expansion in terms of pair potentials. We use five two-particle functions. The interaction of an H₂ molecule with the passivation hydrogen atoms, $V_{\text{H}} = V_1(r)$, the second layer silicon atoms, $V_{\text{Si}_2} = V_3(r)$, and the bulk atoms, $V_{\text{Si}} = V_4(r)$, are described by the repulsion part of the Buckingham potential. For the interaction between H₂ and the first layer silicon atoms we use the Morse potential. The hydrogen intermolecular interaction, $V_{\text{H}_2} = V_5(r)$, is considered within the framework of the conventional Lennard-Jones model with parameters $\epsilon/k_{\text{B}} = 36.7$ K and $\sigma = 2.96$ Å [15]. Thereby the whole set of pair potentials representing the potential function is

$$V_i = A_i \exp(-\beta_i r), \quad i = \{1, 3, 4\}, \quad (11)$$

$$V_2(r) = A_2 [e^{-2\beta_2(r-r_2^*)} - 2e^{-\beta_2(r-r_2^*)}], \quad (12)$$

$$V_5(r) = 4\epsilon [(\sigma/r)^{12} - (\sigma/r)^6]. \quad (13)$$

TABLE II. Fitted parameters for pair potentials. Energy and distance units are (cm^{-1}) and (\AA).

| Parameter | Value | Parameter | Value |
|-----------|----------------------------|-----------|-------------|
| A_1 | 0.6684392422×10^6 | β_1 | 3.452896593 |
| A_2 | 0.3945112757×10^2 | β_2 | 1.248968963 |
| | | r_2^e | 4.264261852 |
| A_3 | 0.4089798283×10^8 | β_3 | 4.426779703 |
| A_4 | 0.5254899653×10^5 | β_4 | 1.537589534 |

The parameters A_i , β_i , r_i^e , and α_i in Eqs. (11)–(13) were determined by fitting to the *ab initio* energy values with the same cutoff radius of 10\AA . They are gathered in Table II. The weighted standard deviation of the final fit is about 10^2 cm^{-1} . Taking into account the level of the *ab initio* theory, the scale of the system under consideration, and the limitations of the pair-potential model we believe that this representation can be used for the molecular dynamics simulations.

2. Structural, thermodynamic, and kinetic properties

Molecular dynamics calculations agree with the suggestions made on the basis of the temperature dependent Raman spectra (see Figs. 4 and 5) that molecular hydrogen within platelets crystallizes at low temperatures. Solid two-dimensional hydrogen forms a monolayer with the hexagonal structure determined by the two opposite passivated silicon surfaces. The corresponding lattice constant is $a_{\text{hex}} \approx 3.84 \text{\AA}$, which implies that the density of H_2 within a “completely filled” platelet is equal to approximately $0.78 \times 10^{15} \text{ cm}^{-2}$. This finding agrees well with the H_2^* -double-layer mechanism of Si{111}-platelets formation [9,10].

Figure 7 shows the radial distribution function of H_2 in the temperature range 50 to 300 K. At 50 K sharp peaks corresponding to the coordination spheres of two-dimensional hexagonal lattice at a_{hex} , $a_{\text{hex}}\sqrt{3}$, $2a_{\text{hex}}$, $a_{\text{hex}}\sqrt{7}$, $3a_{\text{hex}}$, etc. are clearly seen. The peak at around 3.3\AA that appears at higher temperatures corresponds to the parameter σ in Eq. (13). As the temperature rises, the long-range order is disturbed, thereby indicating the presence of a fluid phase. Still, the platelet’s

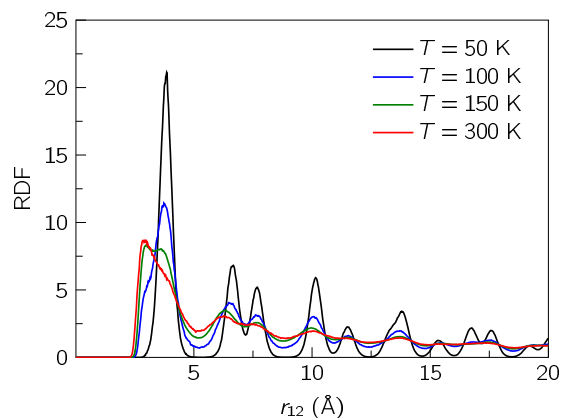


FIG. 7. Radial distribution function of molecular hydrogen within the platelet for different temperatures.

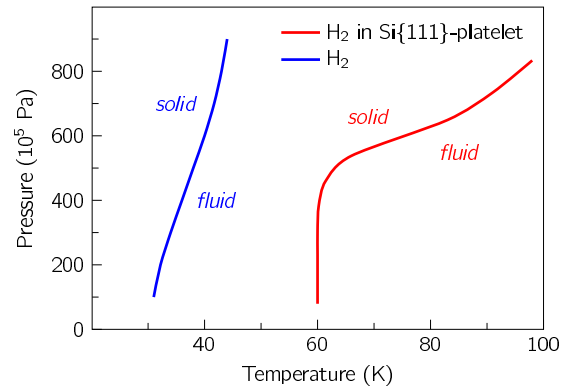


FIG. 8. Phase diagram of H_2 in the platelet and phase diagram of bulk H_2 , simulated with the LJ potential.

structure is detectable via small maxima for a few coordination spheres even at $T = 300 \text{ K}$.

A calculated p - T phase diagram of two-dimensional H_2 is presented in Fig. 8. The maximum pressure corresponds to the completely filled platelet. Since the LJ model is a rather crude approximation, in order to exclude systematic errors of the method and get a direct insight into the influence of the platelet’s structure on the thermodynamic properties of hydrogen a phase diagram of bulk H_2 (hcp structure) with the only intermolecular potential described by Eq. (13) was simulated as well. Comparison with experiment [58] clearly shows that this approach gives reasonable description of the bulk hydrogen behavior.

According to Fig. 8 either the solid or the fluid phase of the two-dimensional molecular hydrogen can exist. We do not distinguish between the gas and the liquid phases since the temperatures under consideration are higher than the critical one.

Another conclusion that follows from the p - T diagram is a noticeable increase of the transition temperature with the pressure starting from around 500 MPa. This finding leads us to the inference that two-dimensional hydrogen crystallizes in the defect-free hexagonal lattice at about 100 K. The conclusions of theory agree very well with the experimental data on the temperature dependence of the $S_0(0)$ Raman transition (see Figs. 4 and 5). There, the FWHM behavior points out towards a phase transition of hydrogen at similar temperatures.

Comparison between the two curves presented in Fig. 8 implies that the thermodynamic properties of confined molecular hydrogen in the platelet are mainly determined by the PES characteristics including the presence of maxima in the vicinity of Si-H terminations rather than intermolecular interaction.

According to our molecular dynamics simulations, the pressure of H_2 within the platelet at room temperature should be about 0.1 GPa (in the case of completely filled platelet). This value is one order of magnitude lower compared to the early estimates deduced from the equation of state of bulk hydrogen [8,11]. To clarify the reason for such a discrepancy the pressure of H_2 gas placed between two parallel elastically reflecting walls was calculated. If only intermolecular LJ interaction is taken into account, the value of pressure becomes 1 GPa. We conclude from here that it is the potential energy surface rather than the two-dimensionality that is responsible for the pressure

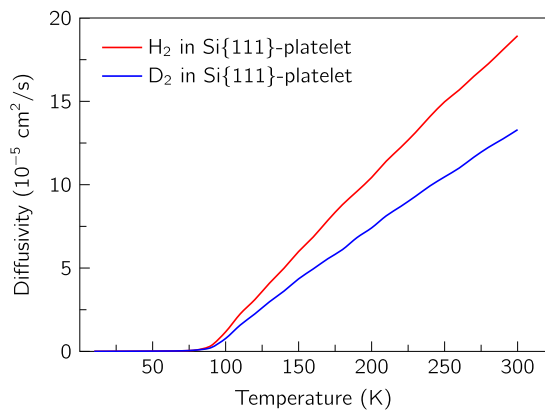


FIG. 9. Temperature dependence of diffusion coefficients for H₂ and D₂ localized within the platelet structure.

lowering obtained. Still, we expect that molecular dynamics simulations slightly underestimate the value since in our model only H₂'s are allowed to move.

Figure 9 shows the calculated diffusion coefficients vs temperature of molecular hydrogen and deuterium within the platelet. According to our simulations the molecules do not penetrate into the bulk of Si. For temperatures above 100 K it can be approximated as $D \sim T^{3/2}/p\sqrt{m}$, i.e., the dependence is inherent in a gaseous state. Note that the diffusion coefficient of hydrogen in platelets lies in between those typical for liquids and gases [54].

3. Rotational states of two-dimensional parahydrogen

Variational calculations reveal that similar to the bulk system the $J = 2$ state at the Γ point of pure parahydrogen ($n_o:n_p = 0:4$) in the platelet splits into a triplet with the energy values of 351.29 ($m = \pm 1$), 357.09 ($m = \pm 2$), and 362.89 cm^{-1} ($m = 0$). Introduction of even a small amount of orthomolecules leads to a significant broadening of the triplet states and consequently to the formation of an energy band with the width of about 15 cm^{-1} .

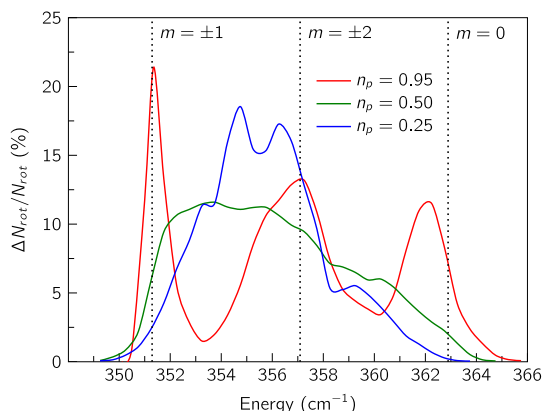


FIG. 10. Density of rotational states of two-dimensional para-H₂ at the Γ point calculated for different ortho-to-para ratios. Three dotted lines represent the rotational states of defect-free solid parahydrogen.

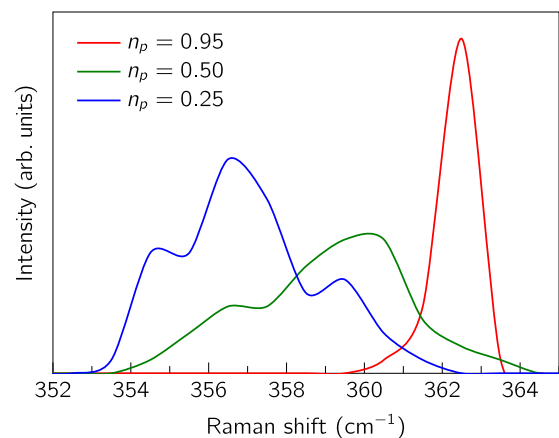


FIG. 11. Calculated integrated intensities for the $S_0(0)$ transition of para-H₂ for different ratios between the ortho- and paraspecies.

Figure 10 shows the density of rotational states of two-dimensional parahydrogen at the Γ point calculated for different ratios between the ortho- and paramolecules. In the case of nearly pure parahydrogen ($n_p = 0.95$) the triplet states are well distinguishable. Since the coherent-scattering regions extend over several unit cells of the two-dimensional lattice, the system substantially inherits the properties of the defect-free crystal.

As the relative amount of ortho-H₂ grows in, the neighborhood of parahydrogen drastically changes, resulting in both violation of the local symmetry and significant reconstruction of intermolecular interaction. As a result, the structure of the rotational energy levels changes. At the same time the wave functions in Eq. (3) turn into the superposition of rotational states with different m values. For the $J = 2$ rotational level perturbed by the EQQ potential, only the $m = 0$ and $m = \pm 2$ states mix up.

According to the selection rules for pure para-H₂ crystallized within the platelet, only the transition to the $J = 2, m = 0$ state is allowed. This is consistent with the low-temperature Raman scattering spectra (see Fig. 5, $T = 19$ K, $n_o:n_p = 0:4$) clearly indicating that the maximum of the $S_0(0)$ line is blueshifted and its FWHM is substantially less as compared to the cases of higher ortho-H₂ concentration (Fig. 4).

Figure 11 shows simulated profiles of the low-temperature $S_0(0)$ Raman transition for different ortho-to-para ratios. For a negligible amount of ortho-H₂, its FWHM is significantly reduced compared to those of the $n_o:n_p = 2:2$ and $n_o:n_p = 3:1$ cases. When the concentration of ortho-H₂ molecules increases, the $S_0(0)$ line both broadens and redshifts, which agrees very well with the low-temperature Raman spectra obtained for the different $n_o:n_p$ ratios (see Figs. 4, 5, and Table I).

To summarize, our theoretical analysis can account for the behavior of molecular hydrogen trapped within {111}-oriented platelets in silicon and explain most of the experimental findings reported in the literature. Based on this we expect that a similar approach can be applied further on to get insight into the properties of hydrogen-induced platelets observed in other semiconductors.

IV. CONCLUSIONS

Molecular hydrogen trapped within {111}-oriented platelets in Si has been studied by means of Raman scattering and first principles theory. The rotational transition $S_0(0)$ of para- H_2 at different sample temperatures has been used as a probe. To explain the temperature dependence of the $S_0(0)$ line shape a comprehensive theoretical investigation has been carried out.

It has been revealed that the phase transition from the fluid to the solid state in two-dimensional molecular hydrogen lying in the {111} plane of silicon occurs approximately at 100 K, i.e., the transition temperature is substantially higher than that of bulk H_2 . The H_2 solid phase in a platelet can be visualized as a hexagonal monolayer with a lattice constant of $a/\sqrt{2}$, where a is the silicon structure parameter.

The shape of the $S_0(0)$ line at helium temperatures strongly depends on the relative content of ortho- and para- H_2 . It is

found to be mainly determined by the properties of hydrogen intermolecular interaction and the system symmetry. The experimental and theoretical findings are in good agreement with each other and allow us to get further insight into the behavior of molecular hydrogen trapped within {111}-oriented platelets in silicon.

ACKNOWLEDGMENTS

This work was supported in part by the Deutsche Forschungsgemeinschaft (Grant No. LA 1397/15). The electronic structure calculations were carried out with the support of the Ministry of Education and Science of the Russian Federation, Project No. 3.9586.2017/8.9. Sergey Yurchenko (University College London, UK) and Igor Chaplygin (Technische Universität Dresden, Germany) are greatly acknowledged for the numerous and fruitful discussions.

-
- [1] S. J. Pearton, J. W. Corbett, and M. Stavola, *Hydrogen in Crystalline Semiconductors* (Springer-Verlag, Berlin, 1992).
- [2] N. M. Johnson, F. A. Ponce, R. A. Street, and R. J. Nemanich, *Phys. Rev. B* **35**, 4166 (1987).
- [3] J. N. Heyman, J. W. Ager III, E. E. Haller, N. M. Johnson, J. Walker, and C. M. Doland, *Phys. Rev. B* **45**, 13363 (1992).
- [4] E. V. Lavrov and J. Weber, *Phys. Rev. Lett.* **87**, 185502 (2001).
- [5] J. R. Botha, R. E. Kroon, and J. H. Neethling, in *Proceedings of Microscopy Society of South Africa*, edited by E. Cloete *et al.*, Vol. 27 (Onderstepoort: Microscopy Society of Southern Africa, South Africa, 1997), p. 37.
- [6] S. Muto, S. Takeda, and M. Hirata, *Mater. Sci. Forum* **196**, 1171 (1995).
- [7] M. Hiller, E. V. Lavrov, and J. Weber, *Phys. Rev. B* **71**, 045208 (2005).
- [8] S. Muto, S. Takeda, and M. Hirata, *Philos. Mag. A* **72**, 1057 (1995).
- [9] S. B. Zhang and W. B. Jackson, *Phys. Rev. B* **43**, 12142 (1991).
- [10] N. Martsinovich, M. I. Heggie, and C. P. Ewels, *J. Phys. Condens. Matter* **15**, S2815 (2003).
- [11] Y.-S. Kim and K. J. Chang, *Phys. Rev. Lett.* **86**, 1773 (2001).
- [12] B. Hourahine, R. Jones, and P. R. Briddon, *Physica B* **376**, 105 (2006).
- [13] G. Herzberg, *Molecular Spectra and Molecular Structure: I. Spectra of Diatomic Molecules* (Krieger, Malabar, 1989).
- [14] E. P. Wigner, *Zeitschrift für Physikalische Chemie B* **23**, 28 (1933).
- [15] I. F. Silvera, *Rev. Mod. Phys.* **52**, 393 (1980).
- [16] A. Driessen, E. van der Poll, and I. F. Silvera, *Phys. Rev. B* **30**, 2517 (1984).
- [17] E. Ilisca and S. Sugano, *Phys. Rev. Lett.* **57**, 2590 (1986).
- [18] M. G. Pravica and I. F. Silvera, *Phys. Rev. Lett.* **81**, 4180 (1998).
- [19] M. A. Strzhemechny and R. J. Hemley, *Phys. Rev. Lett.* **85**, 5595 (2000).
- [20] Y. L. Sandler and M. Gazith, *J. Phys. Chem.* **63**, 1095 (1959).
- [21] E. Ilisca, *Phys. Rev. Lett.* **66**, 667 (1991).
- [22] E. Ilisca and S. Paris, *Phys. Rev. Lett.* **82**, 1788 (1999).
- [23] K. Fukutani, K. Yoshida, M. Wilde, W. A. Diño, M. Matsumoto, and T. Okano, *Phys. Rev. Lett.* **90**, 096103 (2003).
- [24] Yu. Ya. Milenko, R. M. Sibileva, and M. A. Strzhemechny, *J. Low Temp. Phys.* **107**, 77 (1997).
- [25] M. Hiller, E. V. Lavrov, and J. Weber, *Phys. Rev. Lett.* **98**, 055504 (2007).
- [26] M. Hiller, E. V. Lavrov, and J. Weber, *Physica B* **401**, 97 (2007).
- [27] C. Peng, M. Stavola, W. B. Fowler, and M. Lockwood, *Phys. Rev. B* **80**, 125207 (2009).
- [28] V. V. Melnikov and E. V. Lavrov, *Russ. Phys. J.* **59**, 2168 (2017).
- [29] M. Hiller, E. V. Lavrov, and J. Weber, *Phys. Rev. B* **80**, 045306 (2009).
- [30] Edited by D. R. Lide, *CRC Handbook of Chemistry and Physics* (CRC Press LLC, Boca Raton, London, New York, 2001–2002), 82nd ed.
- [31] J. P. Perdew, J. A. Chevary, S. H. Vosko, K. A. Jackson, M. R. Pederson, D. J. Singh, and C. Fiolhais, *Phys. Rev. B* **46**, 6671 (1992).
- [32] J. P. Perdew and Y. Wang, *Phys. Rev. B* **33**, 8800 (1986).
- [33] J. P. Perdew, *Phys. Rev. B* **33**, 8822 (1986).
- [34] R. Dovesi, R. Orlando, B. Civalleri, C. Roetti, V. R. Saunders, and C. M. Zicovich-Wilson, *Z. Kristallogr.* **220**, 571 (2005).
- [35] R. Dovesi, V. R. Saunders, C. Roetti, R. Orlando, C. M. Zicovich-Wilson, F. Pascale, B. Civalleri, K. Doll, N. M. Harrison, I. J. Bush *et al.*, *CRYSTAL09 User's Manual* (University of Torino, Torino, 2009).
- [36] V. V. Melnikov and S. N. Yurchenko, *Russ. Phys. J.* **56**, 1363 (2014).
- [37] V. V. Melnikov, *J. Exp. Theor. Phys.* **120**, 1005 (2015).
- [38] V. V. Melnikov and S. N. Yurchenko, *J. Chem. Phys.* **143**, 164305 (2015).
- [39] F. J. Torres, B. Civalleri, C. Pisani, and P. Ugliengo, *J. Phys. Chem. B* **110**, 10467 (2006).
- [40] T. H. Dunning Jr., *J. Chem. Phys.* **53**, 2823 (1970).
- [41] S. Plimpton, *J. Comp. Phys.* **117**, 1 (1995).
- [42] S. Nosé, *J. Chem. Phys.* **81**, 511 (1984).
- [43] W. G. Hoover, *Phys. Rev. A* **31**, 1695 (1985).

- [44] J. Van Kranendonk, *Physica* **25**, 1080 (1959).
- [45] J. Van Kranendonk, *Can. J. Phys.* **38**, 240 (1960).
- [46] S. S. Bhatnagar, E. J. Allin, and H. L. Welsh, *Can. J. Phys.* **40**, 9 (1962).
- [47] E. J. Allin, A. H. Mc Kague, V. Soots, and H. L. Welsh, *J. Phys.* **26**, 615 (1965).
- [48] T. Oka, *Annu. Rev. Phys. Chem.* **44**, 299 (1993).
- [49] T. Nakamura, *Prog. Theor. Phys.* **14**, 135 (1955).
- [50] J. Van Kranendonk, *Solid Hydrogen. Theory of the Properties of Solid H₂, HD, and D₂* (Plenum Press, New York, 1983).
- [51] V. V. Melnikov, S. N. Yurchenko, P. Jensen, and A. I. Potekaev, *Russ. Phys. J.* **58**, 1040 (2015).
- [52] P. Diep and J. K. Johnson, *J. Chem. Phys.* **112**, 4465 (2000).
- [53] T. Lu and F. Chen, *J. Mol. Model.* **19**, 5387 (2013).
- [54] I. S. Grigoriev, E. Z. Meilikhov, and A. A. Radzig, *Handbook of Physical Quantities* (CRC Press, Boca Raton, FL, 1996).
- [55] B. P. Stoicheff, *Can. J. Phys.* **35**, 730 (1957).
- [56] Edited by M. Cardona and G. Güntherodt, *Topics in Applied Physics*, Vol. 50 of *Light Scattering in Solids II* (Springer, Berlin, 1982).
- [57] D. A. Long, *The Raman Effect* (John Wiley & Sons, Ltd, New York, 2002).
- [58] D. A. Young, *Phase Diagrams of the Elements* (University of California Press, Berkeley, Los Angeles, Oxford, 1991).